Spatial Trends and Drivers of Bedload and Suspended Sediment Fluxes in Global Rivers

Sagy Cohen[1*], Jaia Syvitaki[2], Thomas Ashely[3], Roderick Lammers[4], Balazs Fekete[5], Hong-Yi Li[6]

[1]Department of Geography, University of Alabama, Tuscaloosa, AL, USA

[2]CSDMS/INSTAAR, University of Colorado at Boulder, Boulder, CO, USA

[3]Civil and Environmental Engineering, Virginia Polytechnic Institute and State University, Blacksburg, VA, USA

[4]School of Engineering and Technology, Central Michigan University, Mt. Pleasant, MI, USA

[5]Department of Civil Engineering, The City College of New York, City University of New York, New York, NY, USA

[6]Department of Civil and Environmental Engineering, University of Houston, Houston, Texas, USA

Corresponding author: Sagy Cohen (`sagy.cohen@ua.edu`)

Key Points:

- A new global-scale bedload flux model is introduced within the WBMsed framework.
- Model proformence and sensitivity analyses show strong correspondence to observations and dependence on discharge and river slope parameters.
- Analysis of spatial dynamics in bedload, suspended bed material and washload show complex relationships globally and along river corridors.

Abstract

Bedload flux is notoriously challenging to measure and model. The dynamics of bedload therefore remains largely unknown in most fluvial systems worldwide. We present a global scale bedload flux model as part of the WBMsed modeling framework. Our results show that the model can very well predict the distribution of water discharge and suspended sediment and well predict bedload. We analyze the model's bedload predictions sensitivity to river slope, particle size, discharge, river width and suspended sediment. We found that the model is most responsive to spatial dynamics in river discharge and slope. We analyze the relationship between bedload and total sediment flux globally and in representative longitudinal river profiles (Amazon, Mississippi, and Lena Rivers). We show that while, as expected, the proportion of bedload is decreasing from headwater to the coasts, there is considerable variability between basins and along river corridors. The latter is largely responsive to changes in suspended sediment and river slope due to dams and reservoirs. We provide a new estimate of water and sediment fluxes to global oceans from 2,067 largest river outlets (draining 67% of the global continental mass). Estimated water

discharge (30,579 km3/y) corresponds well to past estimates however sediment flux is considerably higher. Of the total 22 Gt/y estimated average sediment flux to global oceans, 19 Gt/y is transported as washload, 1 Gt/y as bedload and 2 Gt/y as suspended bed material. The largest 25 rivers are predicted to transport over 55% of total sediment flux to global oceans.

1 Introduction

Quantifying Earth's fluvial sediment budget is important for fluvial and coastal geomorphology, ecology, flood analysis, and stream restoration (Best, 2019). Scarcity in sediment data is severe worldwide (Syvitski et al., 2005). The total fluvial particulate load (Qp) is comprised of bedload (Qb), suspended bed-material load (Qsbm) and wash load (Qw) (for definitions see SOM); the bedload portion is notoriously challenging to measure and model (Gomez, 1991; Kabir et al., 2012). Uncertainties in bedload measurements and modeling are particularly acute in large rivers (Ashley et al., 2020) and over large spatial domains (Lammers and Bledsoe, 2018). Use of acoustic sensing techniques for measuring bedload has increased in recent decades (e.g. Nittrouer et al. 2008; Hackney et al., 2020), providing high fidelity information in large rivers. The equipment cost, including deployment and technical expertise, limits the global reach of the methodology.

Modeling bedload can bridge the limited number of observations and offer an analytical framework for scientific studies and predictions. Bedload formulae range from simplified approximations (e.g., Meyer-Peter and Müller, 1948; Parker 1990) to complex physically based numerical models (e.g., Kabir et al., 2012). HydroTrend v.3.0 (Kettner and Syvitski 2008), a basin outlet model, uses a modified version of the Bagnold (1966) bedload flux equation which, like the equation used in this study, is a simplified stream-power model. The Hatono and Yoshimura (2020) global sediment model employs another stream-power/shear-velocity equation. Mean sediment particle diameter and high-fidelity river slope values are often required data layers. MOSART-sediment (Li et al., 2021) is a newly developed large-scale sediment model utilizing a continuous map of median sediment particle diameter over the contiguous U.S. (Abeshu et al., 2021), river slope values derived from the NHDplus database (McKay et al., 2012) and other parameters estimated a priori. Li et al. (2021) invokes the classic Engelund-Hansen equation (Engelund and Hansen, 1967) to simulate the total bed-material load and another empirical formula to separate the total bed-material load into bedload and suspended bed-material load.

Despite a rich research history, large-scale predictions of bedload flux remain elusive (Gomez, 1991; Kabir et al., 2012), given the reliance of these equations on shear stress and near-bed velocity parameters which are difficult to accurately measure or model (Lammers and Bledsoe, 2018). Several recently proposed models have these hydraulic parameters substituted or approximated with other parameters more easily be obtained or predicted (i.e., Syvitski and Saito 2007, Lammers and Bledsoe, 2018, Ashley et al., 2020).

Here we present a new bedload module within the WBMsed global hydrogeomorphic framework (Cohen et al., 2013, 2014). The module is an adaptation of the Lammers and Bledsoe (2018) bedload model, using novel global-scale estimates of bed particle size, river slope, water density and suspended sediment modules. We analyze and map the spatial dynamics of bedload in the context of the total fluvial sediment budget at a global scale. Three rivers (Amazon, Mississippi, and Lena) are used as case studies for understanding down-stream longitudinal dynamics.

2 Methodology

2.1 Modeling Framework

2.1.1 Hydrological Engine

WBMsed is a modular global scale hydrogeomorphic model (Cohen et al., 2013), and an extension of the WBMplus global hydrology model (Wisser et al., 2010), part of the FrAMES biogeochemical modeling framework (Wollheim et al., 2008). WBMplus simulates water balance/transport at the daily time step and as a function of gridded climatic inputs, soil moisture balance, runoff generation mechanisms, and channelized transport. WBMplus is unique in the number and explicitness of anthropogenic factors: dam operation, irrigation (water uptake from rivers, reservoirs, groundwater) and agriculture (impact evapotranspiration). WBMsed sediment modules use discharge and water temperature, simulated respectively by WBMplus and WBM-TP2M (see Miara et al. 2018, Syvitski et al. 2019) within FrAMES.

2.1.2 Suspended Sediment Module

WBMsed uses the *BQART* model (Syvitski and Milliman, 2007) as the governing suspended sediment flux equation. BQART calculates the long term-average suspended sediment ($\overline{Q}_s = BQ^{0.31}A^{-0.5}RT$) based on average water discharge (Q), runoff contributing *A*rea, maximum topographic *R*elief, averaged ground surface *T*emperature, and a catchment parameter ($B = IL(1–T_e)E_h$) that incorporates a glacial erosion factor (I), *L*ithology factor, trapping efficiency of catchment reservoirs (T_e), and a human-influenced erosion factor (E_h). BQART is calculated for each grid cell as a function of these upstream basin characteristics. Daily Q_s predictions to calculate the rating coefficients are based on the Psi equation (Morehead et al., 2003). Detailed description and analysis of WBMsed suspended sediment module is provided in Cohen et al., 2013 and 2014.

2.1.3 Bedload Module

Bedload flux, Q_b (kg/s), is calculated with a modified version of the Lammers and Bledsoe (2018) equation:

$$Q_b = \left[a(\omega - \omega_c)^{1.5} D_s^{-0.5} \left(\frac{Q}{w}\right)^{-0.5}\right] w \text{ ; when } \omega > \omega_c \quad (1)$$

where a is a coefficient ($1.4\text{x}10^{-4}$) (-), D_s is representative grain size (m), Q is discharge (m^3/s), and w is river width (m), ω and $_c$ are specific and critical

stream powers (W/m^2):

$\omega = \frac{gQS}{w}$ (2)

$\omega_{\mathbf{c}} = 0.1\rho\left[(s-1)gD_s\right]^{1.5}$ (3)

where is fluid density (kg/m^3), g is acceleration due to gravity (constant 9.67 m/s^2), S is river slope (m/m), and s is a unitless sediment specific gravity (assumed to be 2.65). In this paper, w and D_s are estimated using empirical expressions derived from databases reported by Ma et al., (2018) and Recking (2019). Taken together, these comprise a total of over 13000 observations of relevant parameters in 56 different rivers spanning four orders of magnitude of grain size (D_s = 40 μm to 20 cm). Width and grain size relations are derived using using mean values for each river. The width relation ($R^2 = 0.71$) is given by:

$w = 2.15\overline{Q}^{0.67}$ (4)

and the grain size relation ($R^2 = 0.9$) is given by:

$D_s = 3.77\left(\frac{\overline{Q}}{W}\right)^{1.42} S^{1.26}\left(\frac{\overline{Q_S}}{W}\right)^{-0.5}$ (5)

where $\overline{Q_s}$ is average suspended sediment (kg/s).

WBMsed simulates daily water density, , as a function of fluid temperature (T_w; °C) calculated using the Thiesen-Scheel-Disselhorst equation (McCutcheon et al., 1993):

$\rho = 1000\left[\frac{1-(T_w+288.94)}{508929.2(T_w+68.12)}\right](T_w - 3.98)^2$ (6).

Q_b is calculated in each grid-cell and time step as a function of updated parameter values. Cell-to-cell Q_b transport is not simulated. Upstream and temporal dynamics are driven by variability in Q, Q_s and T_w. This means that Q_b is solely transport limited as determined. A similar assumption was made by Li et al. (2021) following Engelund and Hansen (1967).

2.1.3 Suspended Bed Material Module

Suspended bed-material flux (SBM; Q_{sbm}; kg/s) is calculated as (Syvitski et al., 2019):

$Q_{\mathrm{sbm}} = \left(\frac{\rho_s}{\rho_s-\rho}\right)\rho\overline{Q}^{\beta} S\left(0.01\frac{\overline{\mu}}{\mu_s}\right)$ (7)

where ρ_s is sediment density (assumed 2650 kg/m^3), $\overline{\mu}$ and μ_s are transport and settling velocities (m/s) respectfully, and β is a bedload rating term (here assumed 1.0). Transport velocity is simulated by the model as a function of channel geometry and discharge (Manning's equation). Settling velocity is calculated as a function of kinematic viscosity ($f[D_s, T_w, \rho_s, \rho]$), D_s, $\rho_s$and ρ. See Syvitski et al. (2019) for details. In this study, Q_{sbm} is used to calculate the wash load as $Q_w = Q_s$ - Q_{sbm}.

2.2 Simulations Setup, Inputs and Postprocessing

Gridded global-scale simulations are conducted at 6 arc-minutes spatial resolution (~11x11km at the equator) and daily time steps between 1960 and 2019. The first 30 years of the simulations (1960-1989) are used as spin-up and are excluded from the analysis. In this study, the simulations are in the model's 'disturbed' mode in which all the anthropogenic processes are included for both the hydrological engine (irrigation, dam flow regulation, water uptake, agriculture evapotranspiration) and suspended sediment module (T_e and E_h). The Q_b and Q_{sbm} modules do not include direct anthropogenic parameters except through modifications to Q and Q_s. The potential significance of this will be discussed later.

The model input datasets are detailed in Cohen et al. (2013); alterations in this study include: precipitation - monthly TerraClimate (Abatzoglou et al., 2018) dataset re-gridded at 10 arc-minutes resolution, partitioned into daily data by computing the daily fraction from the NCEP reanalysis product (Kalnay et al., 1996; Kistler et al., 2001); air temperature - monthly TerraClimate (Abatzoglou et al., 2018) dataset re-gridded at 10 arc-minutes resolution; reservoir capacity – global reservoir and dam database (GRanD v1.3; Lehner et al., 2011); and flow network – 6 arc-minute HydroSTN30 network which a derivative of HydroSHEDS high resolution gridded network from Lehner et al. (2008).

River slope was originally rasterized from the Lin et al. (2020) global river width dataset. Lin et al. (2020) was selected over the GloRS dataset (Cohen et al., 2019) due to its calculated values in coastal reaches (GloRS mostly has a constant minimum value). The original Lin et al. (2020) dataset and the resulting input layer exhibit a high degree of noise, expressed as high levels of fluctuations along river paths (see Figure S1 for the Mississippi/Missouri longitudinal profile). These fluctuations are not realistic. To alleviate this issue, a smoothed river slope raster was generated by 'burning' the 25^{th} percentile slope value extracted for each WBMsed stream network reach into the global river slope input layer (maximum length 200km). See Figure S1 for comparison between the smoothed and original datasets.

Long-term average model predictions are calculated between 1990 and 2019 for all the analyzed parameters. The analysis presented in this paper only includes grid-cells with average discharge greater than 30 m^3/s (total ~10^5 grid-cells). Masking of grid-cells with Q<30 m^3/s reduces known model and input data biases in streams and small rivers and focuses our analysis on reaches of medium to large rivers. A vectorized version of the model's stream network is used for visualization.

3 Results and Discussion

3.1 Model Evaluation

Q and Q_s are compared against average observations in 39 USGS sites where the discharge record is over 20 years (Table S1). Model predictions were strongly

correlated (log-log linear) with R^2 of 0.99 and 0.89 for Q and Q_s respectively (Figure S2; Q_s data range >3 orders of magnitudes). Q and Q_s are also compared to average estimates from the M&F05 database (Syvitski and Milliman, 2007) in 132 global basin outlets: for Q ($R^2 = 0.99$) and Q_s ($R^2 = 0.73$) (Figure S3; Q_s data range >4 orders of magnitudes). The model underpredicts Q compared to both datasets; by 57% for the USGS dataset (Table S1) and 12% for M&F05. Note that the timeframe of each observation point differs and, in most gage sites, cover only part of the modeled 1990-2019 timeframe. Q_s is slightly (5%) underpredicted compared to the USGS data but considerably overpredicted (60%) compared to the M&F05 datasets. The M&F05 dataset can be outdated and are mostly based on a limited number of within river observations. Overall, the results show the robustness of the WBMsed model at predicting Q and Q_s distribution for global rivers, and improvement of the model's current version (stronger validation results compare to recent analyses in Dunn et al. (2019, 2018) and Moragoda and Cohen (2020)). The improvement in the model is due to an increase in accuracy of its hydrological predictions, attributed to recent enhancements to the WBMplus framework, use of higher resolution precipitation dataset (TerraClimate), and enhancements in WBMsed Q_s trapping module. These enhancements include updating the reservoir input to the latest GRanD (v1.3) dataset.

Bedload predictions are more challenging to evaluate. Bedload observations are determined typically from near-instantaneous measurements (e.g., Helley-Smith sampler) or as average across short intervals (e.g., bedload traps or sonar mapping) (Fekete et al., 2021). Due to their time consuming and expensive nature, long-term and continuous bedload monitoring is rare, especially for large rivers. Some model bedload parameters, primarily river slope and particle size, are spatially variable and can result in noisy longitudinal profiles (as discussed later), complicating comparison to observations in discrete locations.

Lammers and Bledsoe (2018) conducted an extensive evaluation of their bedload model against a large dataset of field and flume data and found strong correspondence (R^2=0.75), particularly in the sand fraction (the smallest fraction in their analysis; cf. Figure 4 in Lammers and Bledsoe, 2018). Field data used in Lammers and Bledsoe (2018) is almost exclusively from small rivers and creeks and so its predictive quality when implemented in WBMsed, given its global resolution, temporal averaging, and dominant bed particle size, cannot be readily assumed from their study. We therefore used a subset of a bedload dataset compiled by Islam (2018) to gain a general evaluation of the model implementation within WBMsed. Observations included in our analysis if the difference between observed and predicted Q was <80%. Subsetting based on differences in Q reduces biases in the analysis stemming from location errors and differences in temporal averaging and conditions (e.g. observations are from predominantly high flow conditions). The subset includes 24 out of 44 sites with a range >3 orders of magnitude in average Q and Q_b (Table S2). Results show good agreement ($R^2 = 0.83$; Figure S4), and are similar in shape to the Lammers and Bledsoe (2018) results. The model predicts on average 45.4 kg/s for this

dataset compared to 79.6 kg/s in the observed data (Table S2). While limited, this data comparison is useful given the wide range of observational magnitudes, offering general trends in global bedload.

Predicted suspended bed material load (Q_{sbm}) yields a slightly lower regression ($R^2 = 0.81$; Figure S2) when compared to the bedload observations (Q_b) and higher overall average (141 kg/s). Regression between predicted Q_b and predicted Q_{sbm} in the 24 locations is strong ($R^2 = 0.89$), explained by the mechanistic similarity and connectivity between Q_b and Q_{sbm}, particularly for sand-bed rivers. A strong co-dependence exists between Q_b and Q_{sbm} in fine bed rivers, especially when temporally averaged, and the two equations share several forcing parameters (S, Q, , D_s).

3.2. Sensitivity of Bedload Predictions to Parameters' Distribution

Lammers and Bledsoe (2018) conducted a sensitivity analysis of their bedload equation and found that the Q and S have the highest sensitivity index values (0.25 and 0.2 respectively), followed by w and D_s (~0.1), and $_c$ (<0.05). The sensitivity of the WBMsed global average bedload predictions was conducted by calculating the regression between predicted Q_b and S, Q, w, and D_s for 91,659 grid-cells (with Q>30 m^3/s and Q_b>1 kg/s). Parameter magnitudes were normalized between 0 and 1 to allow for direct comparison, using log-log linear regression due to data skewness.

Results (Figure 1) show the Q_b spatial distribution to most strongly affected by Q, closely followed by S, and w. The model results are least sensitive to D_s. These results are similar to Lammers and Bledsoe (2018) though the differences in the sensitivity of Q_b to the four parameters are quite small. The relatively high sensitivity to D_s and S increase uncertainty in the bedload predictions as these two parameters are the most challenging parameters to estimate/calculate (Figure 2). River slope calculations are highly sensitive to the accuracy and resolution of the Digital Elevation Model (DEM) used, and the spatial alignment between the DEM and the stream network (Cohen et al. 2018). Particle size is challenging to estimate and even represent in a single parameter given its often high spatial variability and actual value distribution within a single sample. Here D_s is considered as a representative riverbed particle size (D_{50}).

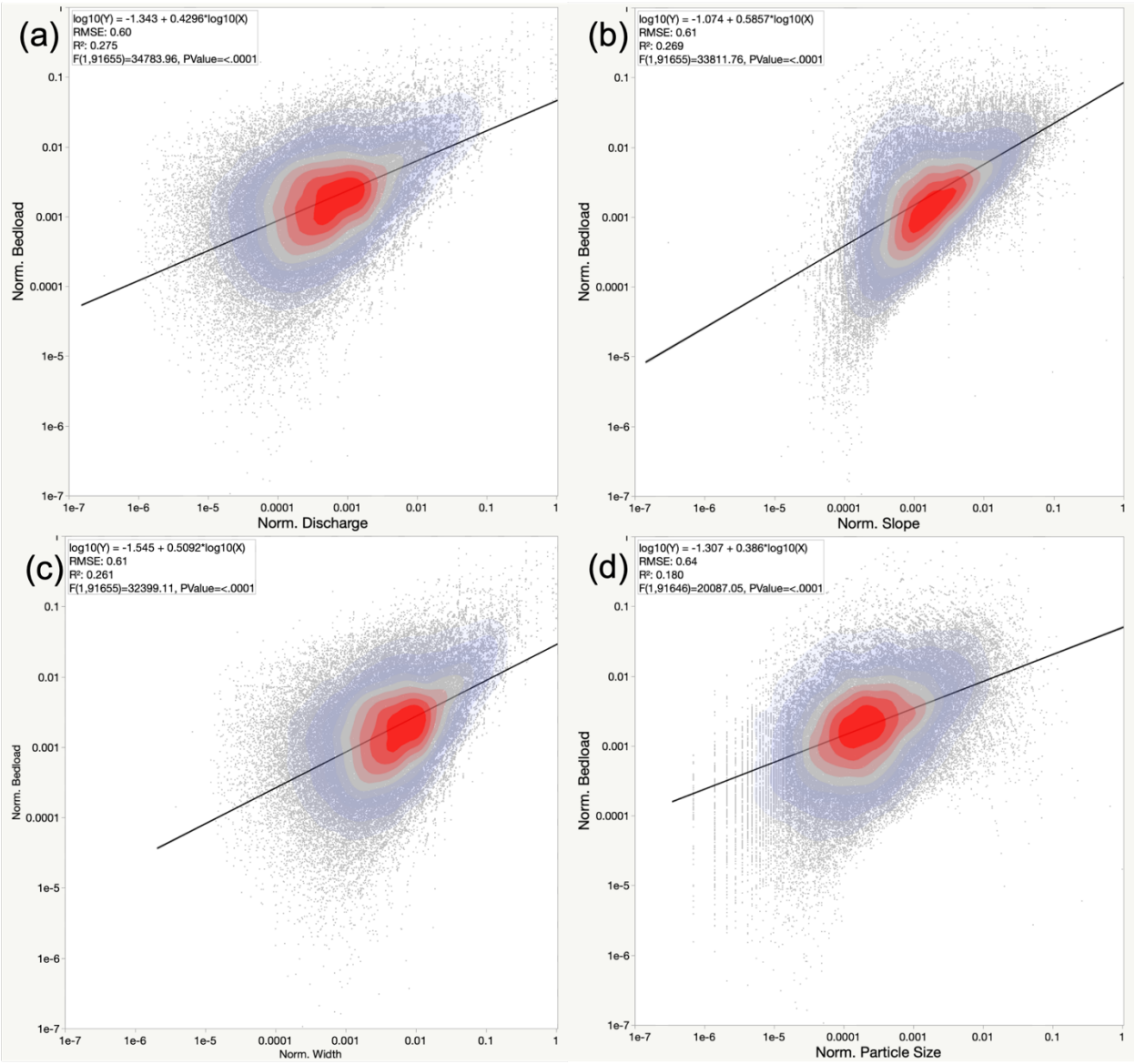

Figure 1. WBMsed model sensitivity plots showing the regression between normalized [0,1] bedload at the modeled domain (91,659 grid-cells) and (a) discharge, (b) river slope, (c) river width, and (d) particle size.

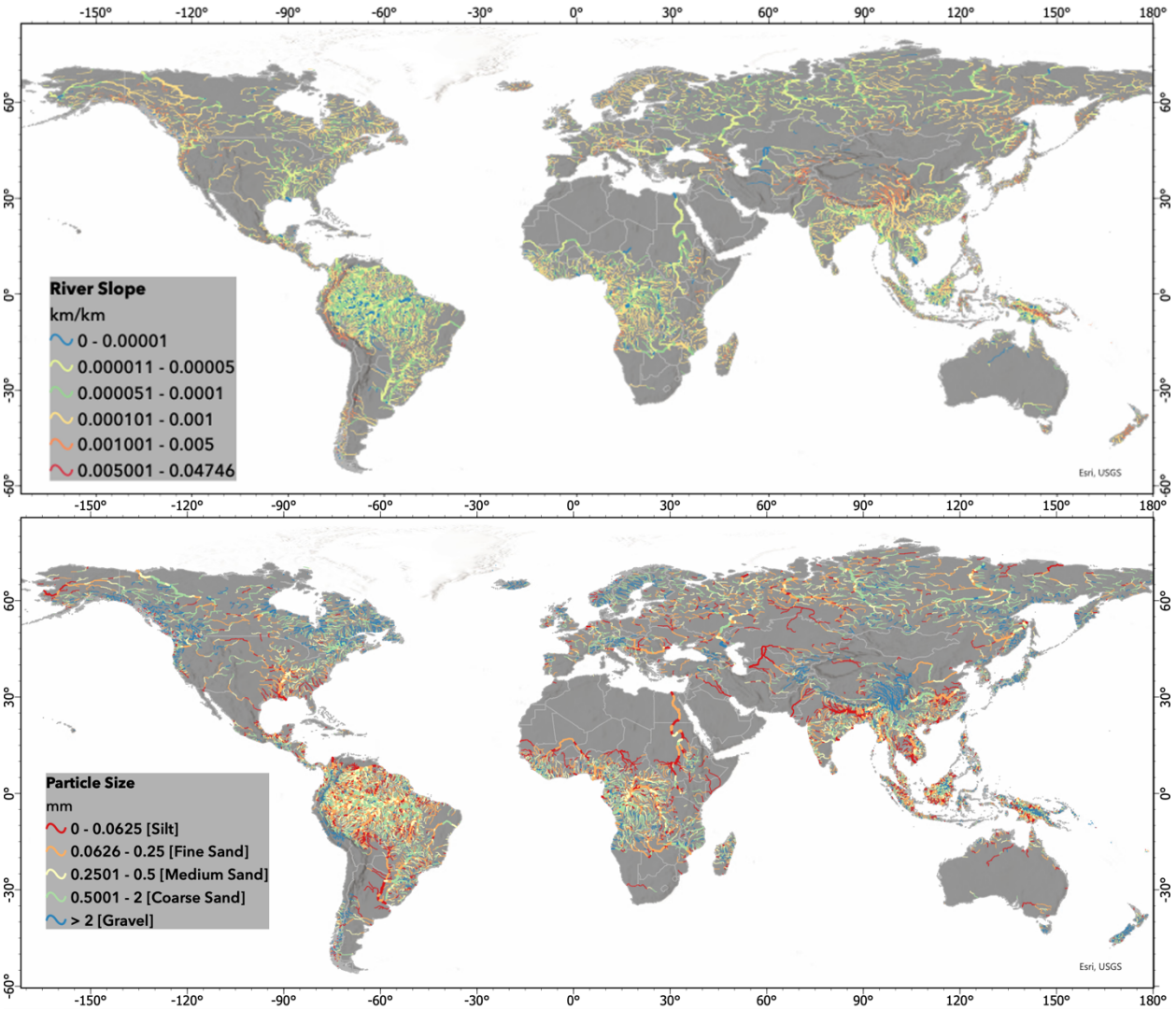

Figure 2. River slope (top) and particle size (bottom) maps. Width of the lines indicates average river-reach discharge.

3.3 Spatial Dynamics and Relationships

Bedload distribution (Figure 3) is highly heterogenous globally, across basins and along main river corridors. High bedload values are prominent in larger rivers and mountainous (headwater) reaches (primarily Himalaya). This duality in bedload distribution stem from the two core drivers of stream power: increasing discharge downstream contrasts with river slope that generally de-

creases downstream (Figure 2). Slope and discharge therefore limit each other at an intra-basin scale. Much of the local spatial variability is attributed to particle size and river slope due to their strong spatial effect on bedload.

The relationship between Q_b and Q_s is also complex. The relationship at a pixel-to-pixel comparison is weak ($R^2 = 0.47$). Q_s values are strongly influenced by upstream basin area and increase in the downstream direction. This leads to contrasting trends with bedload in some locations. Given the complexity in Q_b distribution, latitudinally-averaged values (Figure 4b) show limited variability (<1 order of magnitude) compared to Q_s (>3 orders of magnitude; Figure 4c) with large tropical and mid-latitude rivers dominating the global sediment flux patterns (Figure 3).

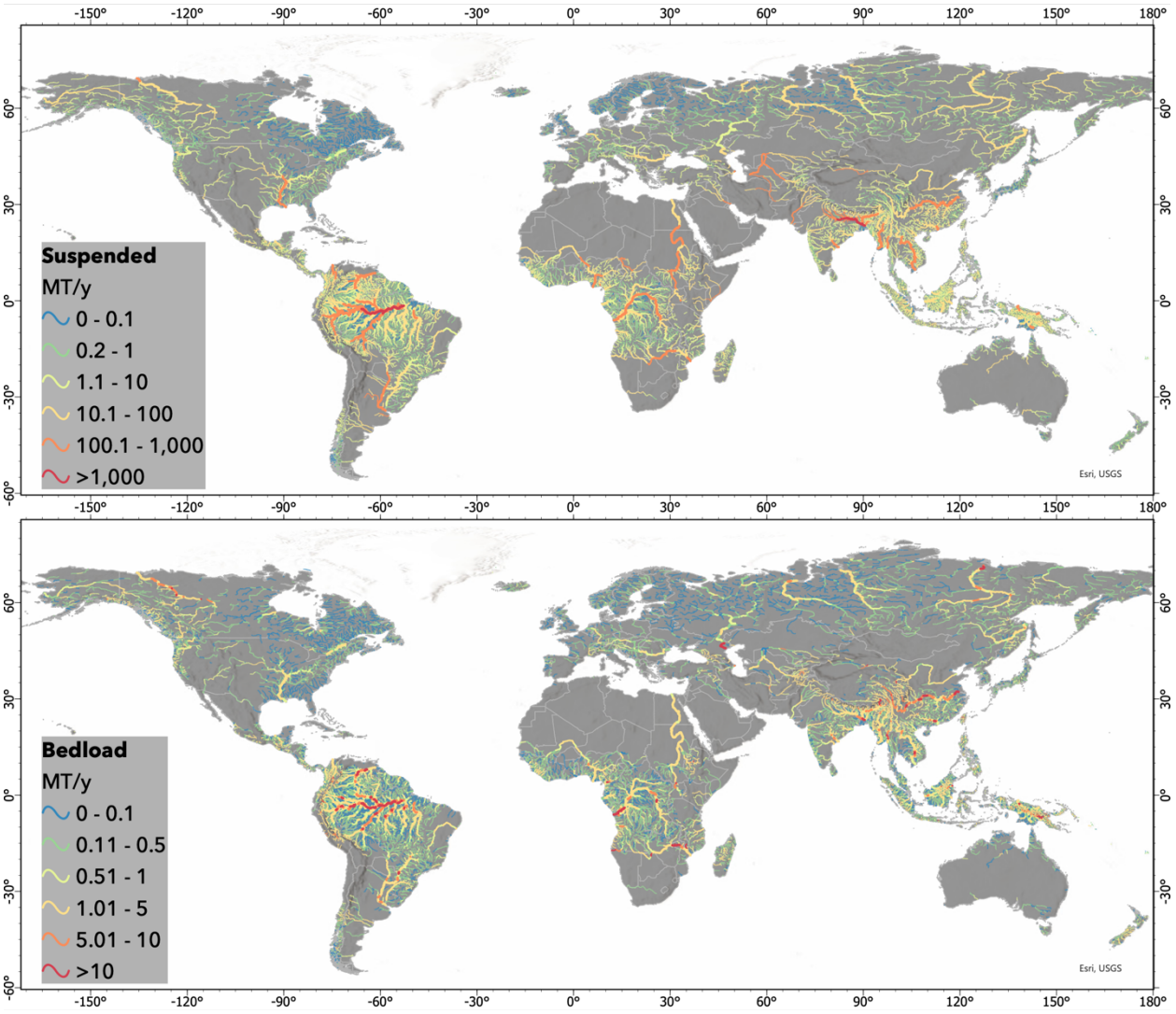

Figure 3. Average (1990-2019) predicted Qs (top) and Qb (bottom) in Mt/y. The width of the lines is indicative of average river-reach discharge. Note differences in color scheme scale.

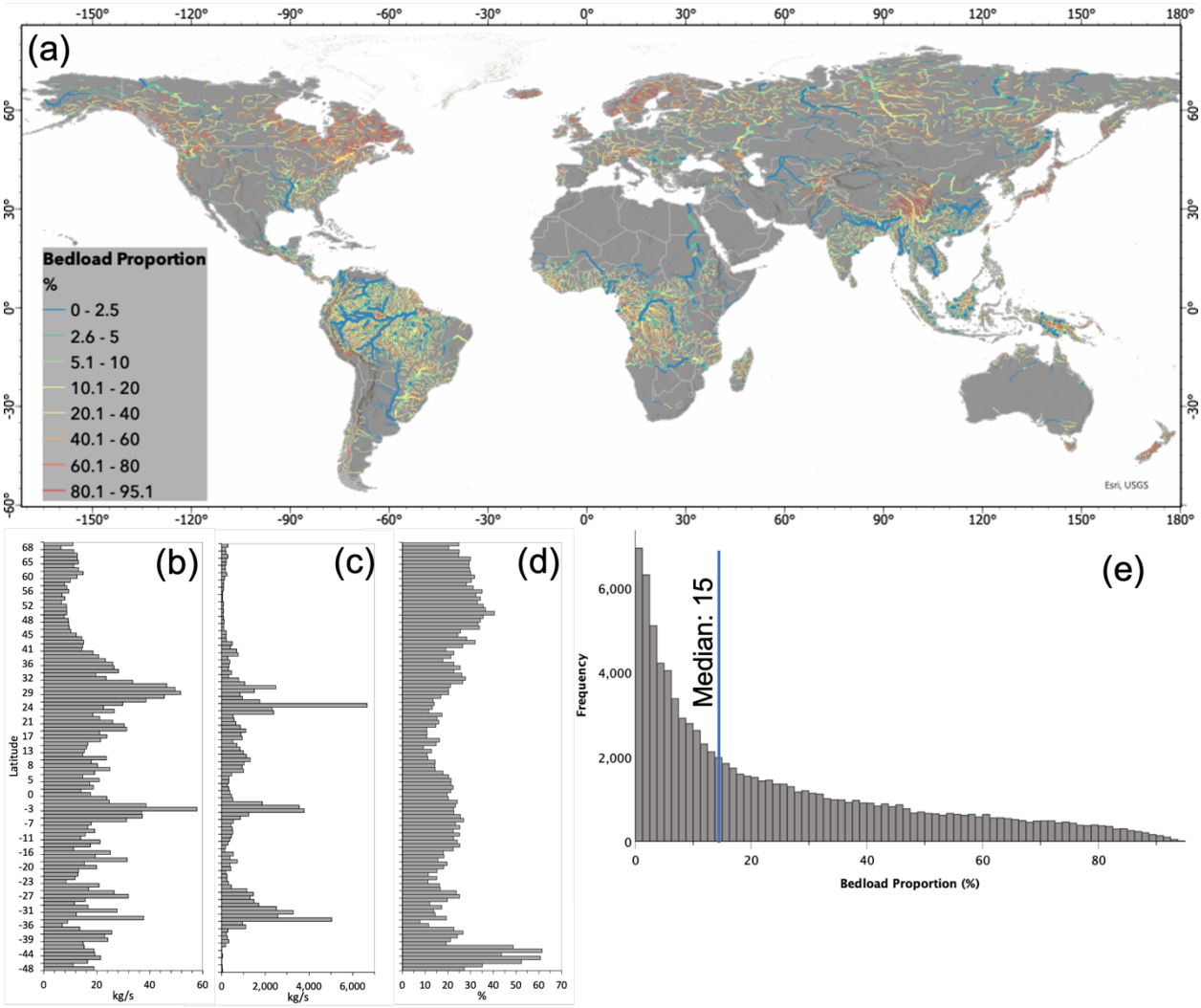

Figure 4. Proportion of bedload flux from total sediment flux (a) map, (b) bedload latitudinal averages, (c) suspended load latitudinal averages, (d) bedload proportion latitudinal averages, and (d) histogram of all grid cells (Q>30 m3/s).

Globally averaged statistics (grid-cells with Q>30 m^3/s) (Table 1) quantify the considerable variability in sediment flux and forcing parameters. For both Q_b and Q_s, the planetary standard deviation greatly exceeds its mean, especially when compared to the median values (Table 1). This further demonstrates the challenges in bedload predictions but also the utility in model simulations that allow for relationship discovery between drivers and other fluvial and environmental factors.

Table 1. Summary statistics for all grid-cells with Q >30 m3/s, Qb > 1 kg/s

(N = 91,659).

	Mean	Median	Std. Deviation
Discharge [m^3/s] (km^3/y)	960 (30)	121 (3.8)	5679 (179)
Suspended [kg/s] (Mt/y)	657 (20)	30 (0.9)	4169 (131)
Bedload [kg/s] (Mt/y)	19 (0.6)	5 (0.15)	55 (1.7)
Suspended bed-material [kg/s] (Mt/y)	64 (2)	24 (0.7)	149 (4.7)
Wash load [kg/s] (Mt/y)	602 (19)	8 (0.2)	4075 (128)
Total sediment load [kg/s] (Mt/y)	676 (21)	41(1)	4195 (132)
Bedload Proportion [%]	24	15	23
Bedload : Suspended load	0.6	0.2	1.2
River slope [km/km]	0.0003	0.0001	0.001
Bed-material particle size [mm]	1.4	0.2	7.8

The proportion of bedload from the total sediment flux (Q_b + Q_s) is low (<2.5%) for large tropical and mid-latitude rivers and high for high altitude rivers and smaller rivers (Figure 4). In high latitudes (>50°), bedload proportion is high (Figure 5d), particularly in small and mid-size rivers (Figure 4a). This latitudinal trend is driven by low Q_s magnitudes in colder river basins, rather than higher bedload magnitudes (Figures 3 & 4b,c). Averaged globally, the model proportion of bedload appears high (mean of 24% and median of 15%; Table 1) compared to historical land-sea estimates (10% Meade et al. 1990; 6.5% Syvitski and Saito, 2007). The high proportion of bedload is located in smaller rivers (which are not weighted by discharge for these statistics) and skew the statistics, but also demonstrate the considerable variability in bedload proportion. Babiński (2005) cataloged the considerable variability in bedload proportion, disputing the commonly referenced range of 1-15%, showing a Q_b/Q_s ratio ranging from 0.3 to 87% in 14 large rivers in Russian and China. Our results show a median Q_b/Q_s ratio of 0.2 (20%), with high mean and standard deviation (Table 1), driven by dominance of small river cells in this analysis.

3.4 River Outlets

The proportion of bedload at river outlets decreases for larger rivers but with considerable variability (note outliers in Figure 5). Once small rivers are filtered out for a discharge-segregated outlet analysis, bedload proportion decreases considerably (Figure 5; Table 2). When considering river outlets with Q>100 m^3/s, thus eliminating more than 50% of river mouths (from 2,067 to 919 outlets), Q_b proportion is reduced to a median of 11% (mean 21%) from 22% (mean 32%). Average bedload proportion is 11% for medium rivers (Q>500m^3/s) and 5.3% for large rivers (Q>2,500 m^3/s), in line with the model estimates of 6.5% by Syvitski and Saito (2007).

Table 2. Statistics for river outlets at 6 discharge filtering brackets. See Figure 6 caption for information about the number of outlets and landmass representation of each bracket. Bedload proportion Sum was calculated from bedload

and total sediment Sum values (in italic).

	Outlet Filter (m^3/s)	**Mean**	**Median**	**Standard Deviation**	**Sum (m^3/s; kg/s)**	**Sum (km^3/y; MT/y)**
Discharge (m^3/s)	>30			,387	,342	,579
	>100			,547	,025	,540
	>500			,169	,703	,710
	>1000			,888	,076	,375
	>2500	,173		,789	,169	,143
	>5000	,756	,373	,315	,914	,662
River Slope (km/km)	>30					
	>100					
	>500					
	>1000					
	>2500					
	>5000					
Particle Size (mm)	>30					
	>100					
	>500					
	>1000					
	>2500					
	>5000					
Susp. Sediment (kg/s)	>30				,035	,973
	>100				,795	,483
	>500			,951	,106	,560
	>1000			,924	,830	,321
	>2500			,393	,864	,840
	>5000	,866		,389	,650	,509
SBM (kg/s)	>30				,348	,565
	>100				,823	,760
	>500				,464	
	>1000				,189	
	>2500				,193	
	>5000				,228	

	Outlet Filter (m^3/s)	**Mean**	**Median**	**Standard Deviation**	**Sum (m^3/s; kg/s)**	**Sum (km^3/y; MT/y)**
Bedload (kg/s)	>30				,302	,145
	>100				,976	
	>500					
	>1000					
	>2500					
	>5000					
Washload (kg/s)	>30				,128	,020
	>100				,688	,966
	>500			,755	,685	,632
	>1000			,668	,493	,554
	>2500			,038	,779	,301
	>5000	,340		,955	,521	,095
Total Sediment (kg/s)	>30				,337	,117
	>100				,772	,144
	>500			,003	,434	,854
	>1000			,991	,414	,560
	>2500			,483	,023	,003
	>5000	,006		,505	,157	,619
Bedload Proportion (%)	>30					*5.2*
	>100					*3.3*
	>500					*1.7*
	>1000					*1.5*
	>2500					*1.2*
	>5000					*0.9*
Bedload/Suspended	>30					*0.055*
	>100					*0.034*
	>500					*0.018*
	>1000					*0.016*
	>2500					*0.012*
	>5000					*0.009*

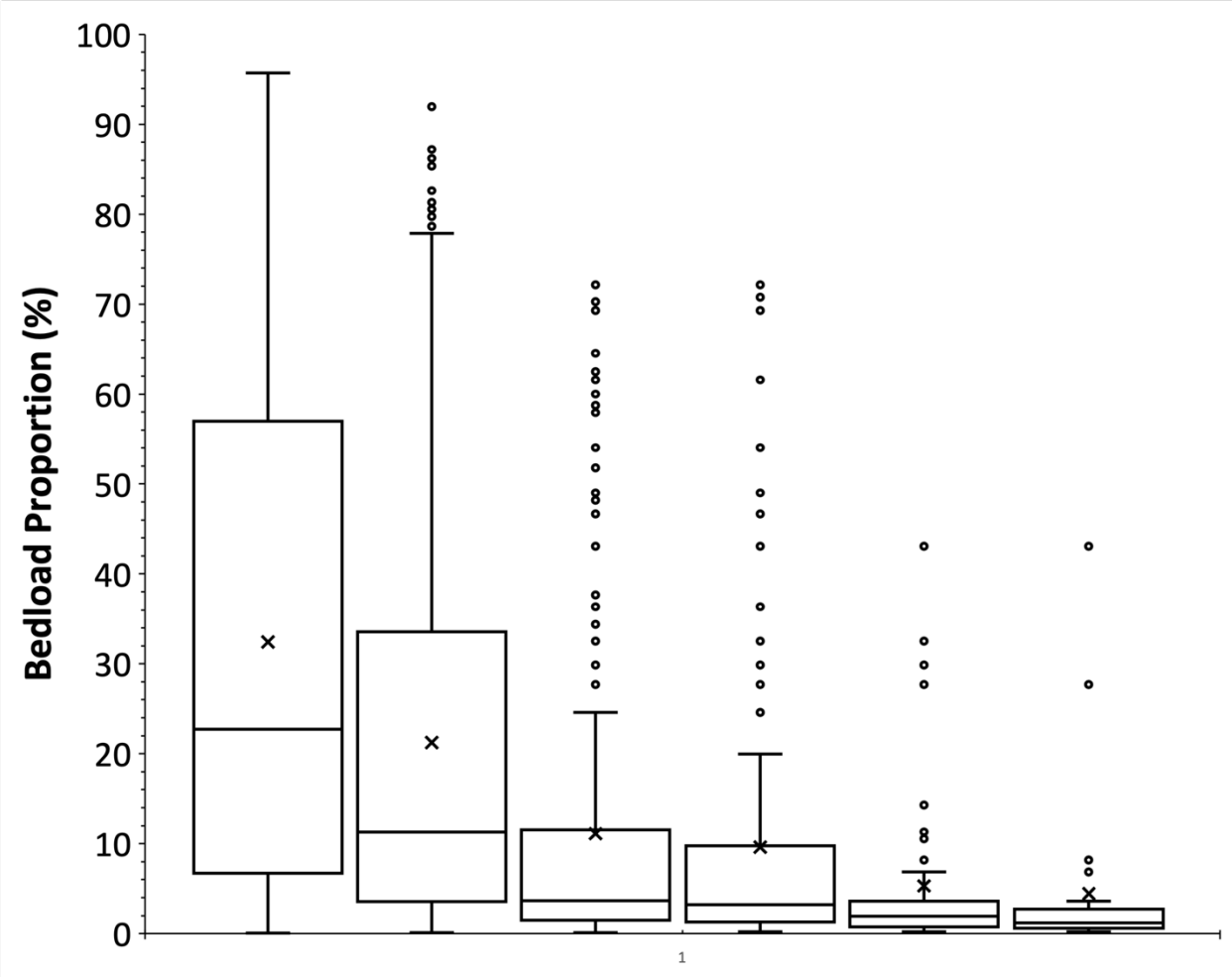

Figure 5. Boxplots of bedload proportion in river outlets to global oceans with average discharge greater than 30 m3/s (n = 2,067, draining 67% of continental land mass (excluding Antarctica)), 100 m3/s (n = 919, draining 60%), 500 m3/s (n = 218, draining 50%), 1,000 m3/s (n = 114, draining 44%), 2,500 m3/s (n = 47, draining 37%), and 5,000 m3/s (n = 25, draining 33%). Black line within the box denotes the median, x denotes the mean and circles are outliers.

Li et al. (2020) provides a recent estimate of Q and Q_s flux to global oceans based on new data and the Milliman and Farnsworth (2011) dataset. Their estimate, based on 1232 rivers for Q and 769 for Q_s, is 31,629 km^3/y and 12,890 MT/y, respectively. These estimates are similar to previous estimates. Our predicted Q (for all 2,067 analyzed outlets where Q>30 m^3/s); draining 68% of continental land mass (excluding Antarctica)), also correspond to the Li et al. (2020) value (30,579 km^3/y; Table 2). Our results further show that half of the

water discharge to global oceans is from the 25 largest global rivers (Q>5,000 m^3/s; draining 33% of continental land mass).

Our Q_s estimate for all analyzed outlets is 47% higher than Li et al. (2020), with a predicted Q_s of 20,973 MT/y. Q_s predictions for the 919 outlets with Q>100 m^3/s, more closely corresponding to the number of outlets (769), is 19,483 MT/y. For the top 25 river outlets (Q>2500 m3/s) predicted Qs is 12,509 MT/y, which closely corresponds to Li et al. (2020). The sum of the model predicted Q_s for the 39 USGS gages used for validation (Section 3.1) is lower than observed Q_s (17,790 and 16,892 kg/s for predicted and observed respectively) but are over predicted for the 128 observations in the M&F05 database (283,509 and 153,376 kg/s for predicted and observed respectively). As discussed earlier, the M&S07 database includes many outdated and partial data, some of which were reused in the Milliman and Farnsworth (2011) database. Given that our predictions (1) correspond well and underpredict USGS observations, (2) are based on nearly 3 times more outlets (2,067 vs. 769), (3) still only represents 68% of Earth's landmass, and (4) underpredict Q, we assert that our new estimate of total sediment flux to global oceans is likely more robust. Our results do not include Greenland which was estimated to have an additional Q_s flux of >1 Gt/y (Overeem et al., 2017). Our predictions however are likely underestimating sediment trapping due to the limited number of dams represented (~7000 large dams compare to ~60,000 reported dams; ICOLD data base 2017).

Bedload flux to global oceans is estimated at 1.1 Gt/y (1145 Mt/y; Table 2). Nearly half of the estimated Q_b is from smaller rivers (30<Q<100 m^3/s; 1,148 out of 2,067 analyzed outlets). Bedload flux from the top 25 largest rivers (Q>5,000 m^3/s) is only 111 Mt/y (<10% of the total flux). These contrasting results from Q_s are due to the much lower river slope in large rivers (by over an order of magnitude) compared to all other outlets (Table 2). Median particle size is relatively consistent for all river size brackets (Table 2).

Total sediment flux (Q_s + Q_b) to global oceans is predicted here to be 22 Gt/y (22,117 Mt/y) for all analyzed outlets. The 25 largest rivers contribute nearly half, with a total sediment flux of 12,619 MT/y, driven by Q_s. Washload (Q_s – Q_{sbm}) to global oceans is predicted to be 19 Gt/y (19,020 MT/y) with the 25 largest rivers contribute over 60%, with a total sediment flux of 12,095 Mt/y.

The proportion of bedload in global sediment flux to global oceans is calculated in Table 2 (rightmost column) as the ratio between total sediment flux and bedload flux in each bracket. This calculation differs from the mean, median and standard deviation reported in Table 2 and Figure 5 as these are raw bedload proportion statistics for all the outlets in each bracket, not taking into account the relative amount of sediment in each (i.e., an outlet for a small river is equally weighted). The proportion of bedload for all analyzed outlets is 5.2%. Larger rivers have considerably lower bedload proportion, with the largest 25 rivers having a value of 0.9%.

3.5 Longitudinal Profiles

Spatial dynamics and trends along longitudinal profiles are analyzed for three rivers:

- Mississippi/Missouri (Figure 6) - ~4,700 km north to south flow, covering over 10° latitude with substantial anthropogenic modification including large dams and long reservoirs.
- Lena/Vitim (Figure 7) - ~4,500 km south to north flow, covering over 20° latitude (50° -70°), limited in-stream modifications (e.g., no dams), complex topographic profile.
- Amazon/Marañón (Figure 8) - ~4,300 km west to east flow, minimal latitudinal range and in-stream modifications.

The Mississippi/Missouri profile shows a sharp increase in Q_s from headwater to the coast, ranging ~5 orders of magnitude, and primarily driven by water discharge. Q_s fluctuates in response to damming (sharp drops, e.g., Canyon Ferry dam in km 350; Figure 6) and to tributary confluences (steep rise; Ohio River at km 3,400). Bedload has a comparatively smaller range, ~2 orders of magnitude, with a weak increasing trend downstream, and considerable fluctuations driven primarily by changes in river slope (Figure 6b, c). The Q_b proportion has a distinct logarithmic decay shape. River slope explains 80% of the variability in bedload proportion (Figure 6d) and, in conjunction with Q_s fluctuations due to dam trapping, can be inversely proportional to Q_s. Dams have contrasting effects on bedload proportion. By reducing Q_s, dams lead to an increase in bedload proportion (see two highlighted regions in the model of Figure 6) as the model does not yet include a bedload trapping component. However large reservoirs reduce a river's surface slope (DEMs record water rather than bed elevation), and this translates to a lower Q_b (most up and downstream highlighted regions in Figure 6). The overall impact of these two effects depends on the degree by which reservoir water slope is captured in the river slope data layer and the length of the reservoir. In WBMsed, sediment trapping behind dams is calculated at the dam location and thus, in long reservoirs, the decrease in Q_s will be predicted considerably downstream from the reservoir intake (where Q_s decrease actually starts). This spatial mismatch is observed in the most-downstream highlighted region in Figure 6, where the ~200 km long Lake Frances results in a considerable drop in river slope and bedload, but its impact on Q_s is predicted downstream of the dam. Immediately upstream and downstream of Lake Frances Case, are two section of elevated bedload proportion. These are driven by high river slope and drop in Q_s due to the dams.

Except for these dam/reservoir-driven fluctuations, bedload proportion is very low for much of the river flow length (less than 5% after km 750). At the lower Mississippi (the most downstream 750 km or so), bedload proportion is around 1%. This is driven by the very low river slope and very high Q_s. Bedload predictions (red star in Figure 6) for the lower Mississippi are underpredicted compared to observation reported by Nittrouer et al. (2008), ~20 vs. ~70 kg/s. Q_s corresponds well with average Q_s observed at the USGS Thebes, IL gage

site (observed 2,550 kg/s; predicted 2,346 kg/s) ~1,000 km upstream of the coast (green star in Figure 6). This suggest that bedload proportion is under predicted at the lower Mississippi River.

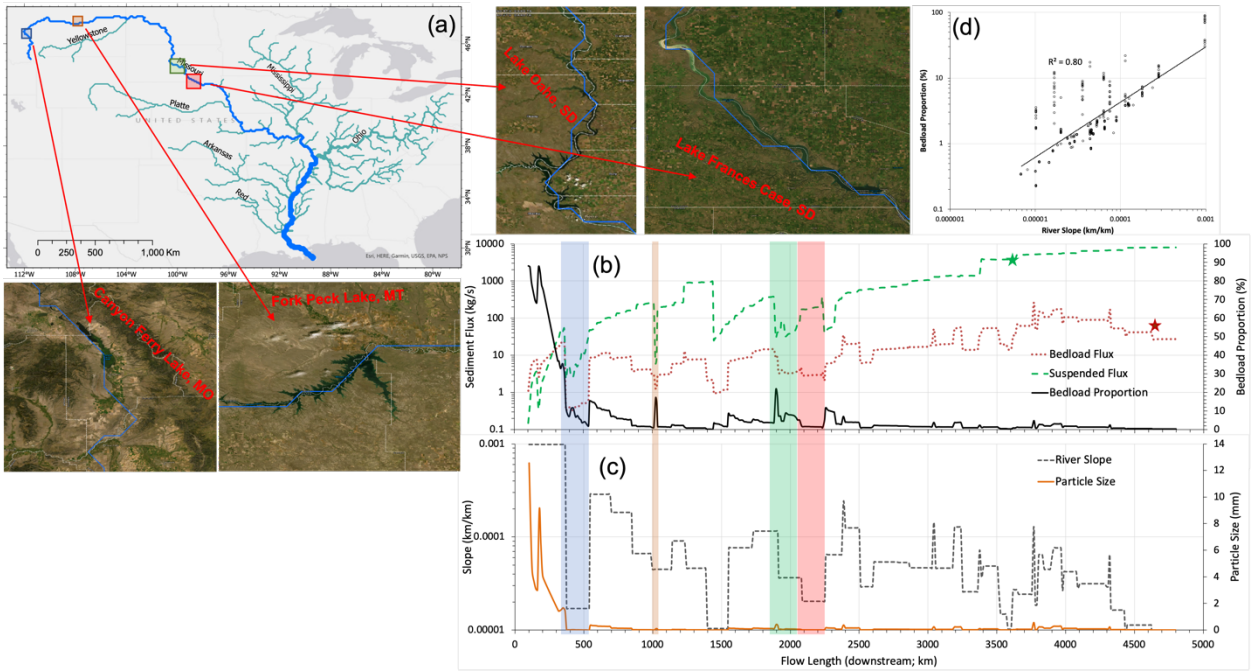

Figure 6. Mississippi/Missouri longitudinal profile (a) map, (b) bedload (kg/s), suspended load (kg/s) and bedload proportion (%), (c) river slope (-) and average bed-material grainsize (mm), and (d) relationship between river slope (-) and bedload proportion (%). Colored bars on (b) and (c) correspond to boxes in (a) and the satellite imagery panels. Green star in (b) is observed Qs from gage site USGS 07022000 Mississippi River at Thebes, IL (2550 kg/s); brown star is observed bedload from Nittrouer et al. (2008).

The Lena/Vitim downstream profile of Q_s shows a relatively steady increases from headwater to the coast (2+ orders of magnitude) and a fluctuating Q_b, driven by river slope, with a general downstream increasing trend (Figs. 7b, 7c). The bedload proportion along the Vitim River (flow length 950–1,100 km; blue highlight in Fig. 7) sharply increases as the river flows through the Kodar Mountain Range in a relatively narrow valley with high slopes. The lowered Q_s across this narrow valley is an artifact of how upstream relief is calculated in WBMsed, particularly in narrow valleys where the coarse grid-cell can capture the surrounding topography. Another zone of higher bedload proportion occurs in the middle of the profile (2,300 – 2750 km; green highlight Fig. 7) wherein river slope and Q_b are elevated. This section of the Lena River, downstream of the confluence with the Olekma River, is narrower and straight flowing with nearly no meandering and braiding. Downstream of this section, the river widens

and bedload is sequestered.

The coastal section of the Lena River has a predicted Q_b of ~200 kg/s (6 Mt/y), driven by high river slope. Q_b is underpredicted compared to a reported value of 14.9 Mt/y; Q_s is overpredicted with 75 Mt/y predicted vs. 21 Mt/y observed (Fofonova et al., 2017), though these observations do not match the timeframe of our results. As a result, bedload proportion (~10%) on the lower Lena is likely considerably underpredicted. Babiński (2005), using several observation references, reported bedload proportion of 43% (Q_b = 17.45 Mt/y, Q_s = 22.6 Mt/y). Model predictions for the Lena River are particularly challenging given its extreme flow regime. Similar to other arctic rivers, the Lena is frozen with very low discharge for much of the year, with spring flooding (to 120,000 m^3/s in a few days) and moderate flows in the summer (~20,000 m^3/s; Rachold et al., 1996). The very energetic annual spring floods were speculated to yield a bedload that exceeds the suspended load at the delta (Are and Reimnitz, 2000).

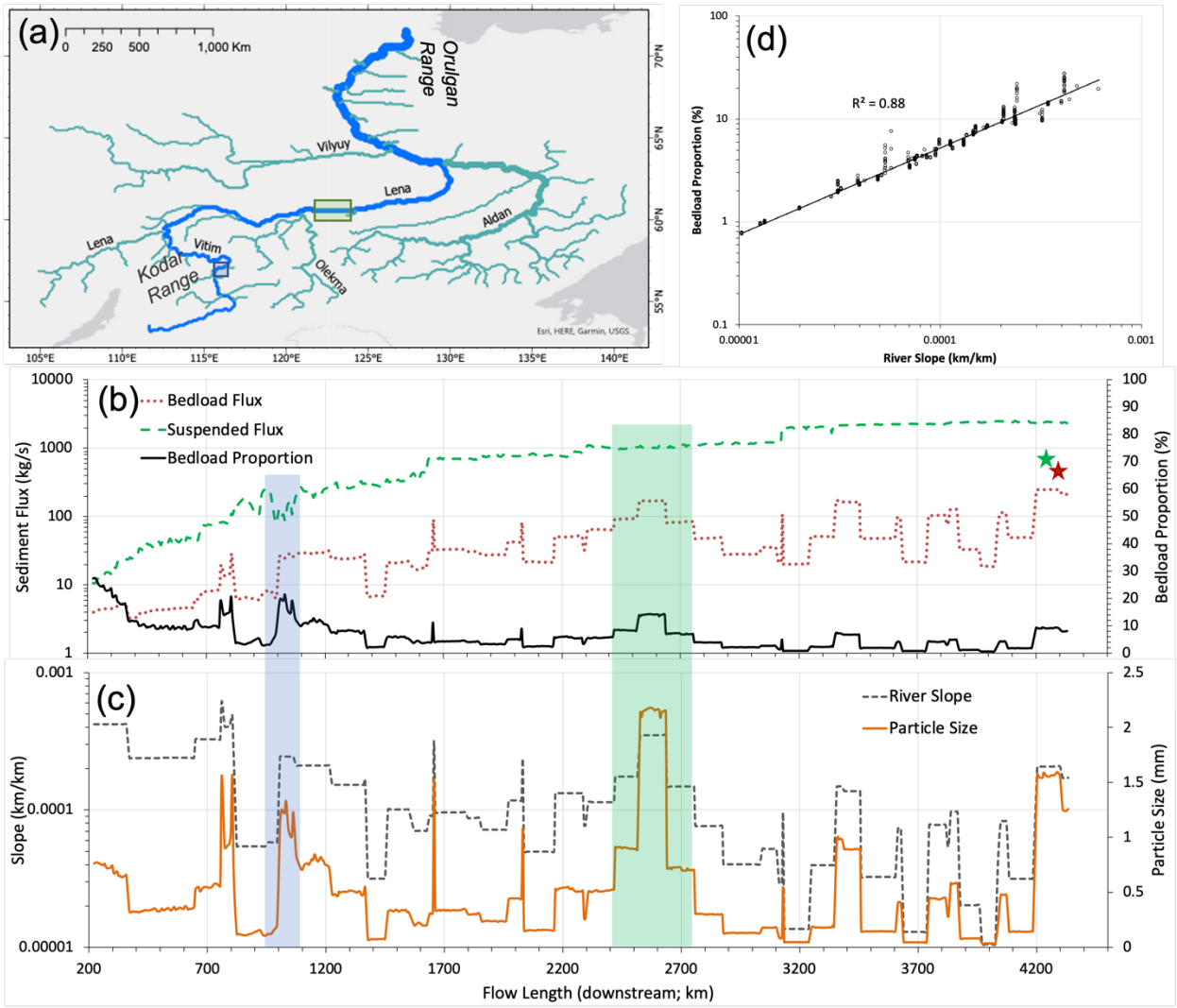

Figure 7. Lena/Vitim longitudinal profile (a) map, (b) bedload (kg/s), suspended load (kg/s) and bedload proportion (%), (c) river slope (-) and size-average bed-material grainsize (mm), and (d) relationship between river slope (-) and bedload proportion (%). Colored bars on (b) and (c) correspond to boxes in (a). Green star in (b) is average of reported SSF range at Kyusyr (11.8 to 21 Mt/yr; Are & Reimnitz, 2000); Brown star is observed bedload at Kusur GS reported by Fofonova et al. (2017).

The Amazon/Marañón profile Q_s increases downstream by over three orders of magnitude (Figure 8b). The Q_b profile shows more localized fluctuations with a very slight increasing trend downstream. Localized spikes and drops in bedload are driven by river slope (Figure 8c,d) attributed to noise in the input layer.

The balancing effects of discharge, particle size and river slope on Q_b are most clearly seen in this profile; slope decreases considerably downstream (~3 orders of magnitudes), while Q_b remains relatively consistent. Particle size decrease from ~6 mm in the upstream reaches to <0.2 mm downstream of the 600 km mark in Figure 8c (see also Figure 3). The 600 km mark is the transition from the Marañón's high altitude Andean valley section to the lower floodplains (Fig. 9c). Bedload proportion drops dramatically from >30% upstream to <5% downstream of the Marañón's transition. At the lower Amazon, bedload proportion is very low (~1%), consistent with reported estimates (Babiński, 2005). Bedload proportion is, however, likely underpredicted due to overprediction of Q_s by the model (green star in Figure 8b).

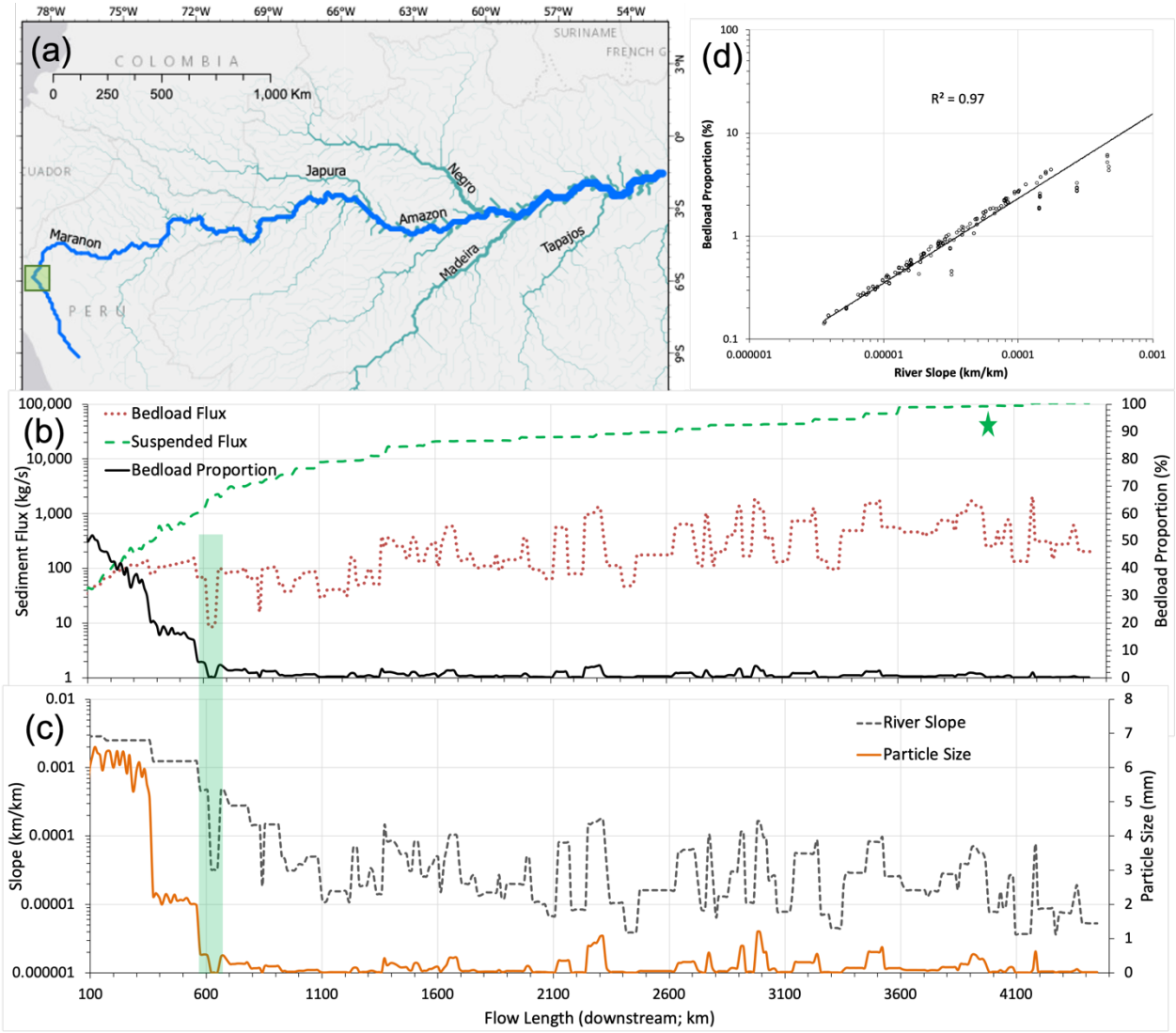

Figure 8. Amazon/Marañón longitudinal profile (a) map, (b) bedload (kg/s), suspended load (kg/s) and bedload proportion (%), (c) river slope (-) and size-average bed-material grainsize (mm), and (d) relationship between river slope (-) and bedload proportion (%). Colored bar on (b) and (c) correspond to boxe in (a). Green star in (b) is a range of observed SSF at Óbidos summarized in Montanher et al. (2018).

Comparison of normalized elevation and bedload proportion for the three longitudinal profiles (Figure 9) offers several insights. Away from the headwaters, bedload proportion drops dramatically by 80%, 70% and 80% within 10% of the downstream flow length (0.1 in Figure 9 x-axis) for the Mississippi/Missouri,

Lena/Vitim and Amazon/Marañón, respectively. The Missouri River shows considerable variability in bedload proportion due to mainstem river dams. Further downstream, the bedload proportion of the Mississippi/Missouri is quite similar to the Amazon/Marañón, with very low values. The Lena/Vitim, while having an elevation profile similar (albeit more complex) to the Mississippi/Missouri, has a different bedload proportion profile. The Amazon/Marañón is unique in that that its bedload proportion profile closely aligns with its elevation profile. This is attributed to the low anthropogenic modification, and relatively homogenous topography, climate, and inter- and intra-annual flow regime. The Lena/Vitim has very low anthropogenic modifications but also extreme seasonal streamflow fluctuations, complex topography, and considerable climatic gradient from headwater to the coast.

This comparison highlights the impacts of anthropogenic modifications, topographic characteristics, climatic gradient/heterogeneity, and flow regime on longitudinal variability in bedload. Q_b dynamics is considerably more complex than Q_s profiles, undermining the assertion that Q_b can be deducted/derived from Q_s alone. Our analysis highlights the need for increased accuracy for two key Q_b driving parameters: primarily river slope and particle size.

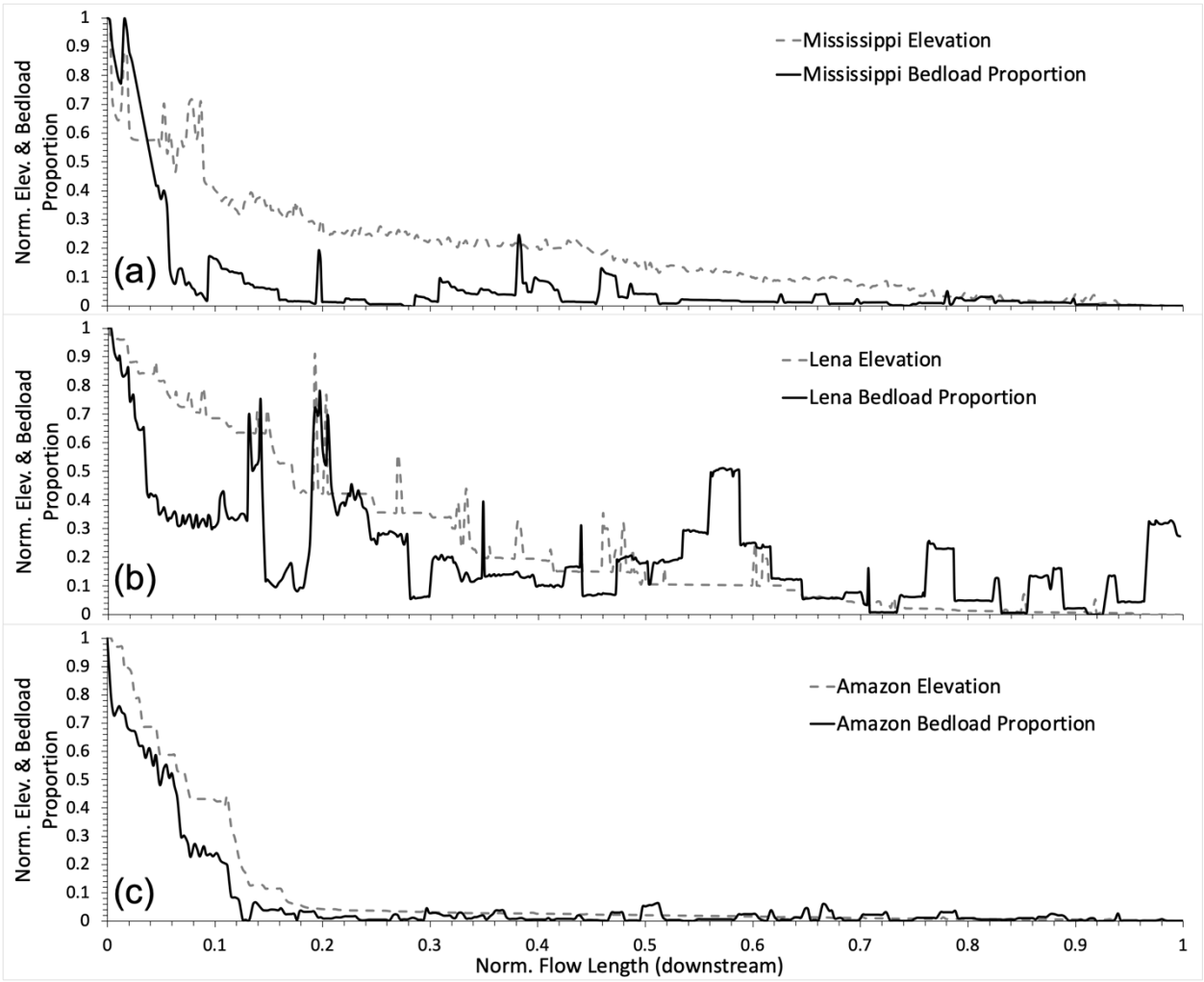

Figure 9. Normalized [0,1] bedload proportion and elevation profiles along a normalized longitudinal profile for (a) Mississippi/Missouri, (b) Lena/Vitim, and (c) Amazon/Marañón.

4 Discussion and Conclusions

New bedload (Qb) and suspended bed material flux (Qsbm) modules are introduced within the global-scale WBMsed hydrogeomorphic model. Global-scale modeling of bedload is enabled by simplified equation parameterizations proposed by Lammers and Bledsoe (2018) and Syvitski et al. (2019). The analysis presented here is based on long-term average (1990-2019) model predictions at 6 arc-minute spatial resolution for grid cells with average discharge larger than 30 m3/s. WBMsed captures discharge and suspended load (Qs) but has a more moderate level of predictive capability for Qb. There remains a scarcity

of bedload evaluation data at the global scale (unlike Q and Qs observations), hindering a robust validation analysis.

Bedload predictions are highly sensitive to discharge, slope, channel width and riverbed particle size. In this study, an improved global river slope dataset and a novel particle size calculation equation are used. However, the grain size predictions are ideal or generalized. They do not include local lithology, and they do not include geological lags from prior climates or deglacial conditions and Earth's ability to return to an equilibrium state. Paraglacial conditions remain in place for many parts of the Arctic (Forbes & Syvitski 1995). Recent advancements in global-scale DEM resolution, accuracy, and processing tools (e.g., Google Earth Engine) can be utilized for improving river slope calculations. Emerging datasets and analysis technuqes can also be used to improve particle size predictions. Abeshu et al. (2021), for example, present a very promising particle size database for the U.S. based on extensive data mining and machine learning analysis.

Perhaps the larger concern comes from our modeling capability versus the speed that we are altering our planet. Mining of sand and gravel from coasts and rivers has reached ~40 Gt/y (Peduzzi, 2014), more than the total fluvial sediment load. Fluvial sand being more angular is much preferred in concrete production compared with rounded particles found on many coastal beaches or desert dunes. As a consequence, riverbed mining is now global, greatly reducing fluvial bed-material transport. 55 Mt/y of aggregates are extracted from the lower Mekong (Bravard et al., 2013), an order of magnitude higher than the down-river transport of sand at 6.2 Mt/y, with riverbank and coastal erosion being the result (Hackney et al., 2020).

Model predicted Qb is spatially heterogenous both between and within basins. The proportion of bedload out of the total particulate flux is very low in large rivers and high in smaller rivers and high latitude rivers. Average bedload proportion for all analyzed grid-cells is 24% but with considerable variability. In the 25 largest global river outlets (Q >5000 m3/s), average bedload proportion is 4.4% (median of 1.2%) and the proportion of bedload exported (by mass) from these rivers is 0.9%.

We offer new estimates of average modern sediment discharge to global oceans. While estimated water discharge values closely match recent published values, our sediment flux values exceed past assessments. We assert that our results are more realistic given: (1) the robustness of the model Q and Qs predictions, (2) our analysis is more extensive in terms of number of rivers modeled, (3) still represents just ~70% of Earth's landmass, and (4) the model underpredict Q. Water discharge to global oceans (1990–2019) is predicted to be 30,579 km3/y, over half of which is from Earth's 25 largest rivers. Qs to global oceans is predicted to be 20,973 Mt/y, nearly 60% of which is from the 25 largest rivers. Washload (Qs – Qsbm) to global oceans is predicted to be 19,020 MT/y with the 25 largest rivers contribute over 60%, (12,095 MT/y). Qb to global oceans is predicted to be 1,145 MT/y, with only ~10% of which is from the 25 largest

rivers. Total sediment flux to global oceans is predicted to be 22,117 Mt/y (22 Gt/y), 57% of which is from the 25 largest rivers.

Analysis of longitudinal profiles of the Amazon/Marañón, Mississippi/Missouri, and Lena/Vitim Rivers, showed that spatial dynamics in bedload is strongly controlled by river slope and is thus very sensitive to noise in its input dataset. Comparison between the three profiles, show that anthropogenic modifications (dams and reservoirs) and topographic features have localized and downstream-propagating impacts on bedload. Climatic gradient and flow regime also influence trends in bedload (and thus Qb proportion). This analysis further demonstrated the complexity of intra-basin bedload dynamics and thus the futility in estimating it based on Q or Qs alone at these scales. It also demonstrates the need to enhance the representation of riverbed particle size and river slope, as it was found to be the primary source of the uncertainty in the model predictions.

Acknowledgments

SC thank the National Science Foundation Geography and Spatial Sciences (GSS) Program for initial funding of this project (Grant 1561082).

Open Research

The model results are available at: https://sdml.ua.edu/datasets-2/. The WBMsed core model code is available on the CSDMS model repository https://csdms.colorado.edu. The WBM framework code is available at its GitHub repository https://github.com/bmfekete/WBM20.

References

Abatzoglou, J.T., S.Z. Dobrowski, S.A. Parks, K.C. Hegewisch, 2018, Terraclimate, a high-resolution global dataset of monthly climate and climatic water balance from 1958-2015, Scientific Data,

Abeshu, G. W., Li, H.-Y., Zhu, Z., & Leung, L. R. (2021). Median bed-material sediment particle size across rivers in the contiguous U.S. *Earth Syst. Sci. Data Discuss.* https://doi.org/10.5194/essd-2021-201

Ashley, T. C., McElroy, B., Buscombe, D., Grams, P. E., & Kaplinski, M. (2020). Estimating bedload from suspended load and water discharge in sand bed rivers. *Water Resources Research*, *56*(2), e2019WR025883.

Are, F., & Reimnitz, E. (2000). An overview of the Lena River Delta setting: geology, tectonics, geomorphology, and hydrology. *Journal of Coastal Research*, 1083-1093.

Babiński, Z. (2005). The relationship between suspended and bed load transport in river channels. W: Sediment Budgets 1. IAHS Publ.

Bagnold, R.A. (1966). An approach to the sediment transport problem from general physics. *US Geological Survey Professional Paper* 422, 1–37.

Best, J. (2019). Anthropogenic stresses on the world's big rivers. *Nature Geoscience,* 12 (1): 7–21.

Bravard, J. P., Goichot, M., & Gaillot, S. (2013). Geography of sand and gravel mining in the Lower Mekong River. First survey and impact assessment. *EchoGéo*, (26).

Cohen, S., A. J. Kettner, J.P.M. Syvitski, and B.M. Fekete (2013), **WBMsed, a distributed global-scale riverine sediment flux model: Model description and validation.** *Computers & Geosciences*, 53: 80–93. doi: 10.1016/j.cageo.2011.08.011

Cohen,S., A. J. Kettner, and J.P.M. Syvitski (2014), **Global suspended sediment and water discharge dynamics between 1960 and 2010: Continental trends and intra-basin sensitivity.** *Global and Planetary Change*, 115: 44-58.

Cohen, S., Wan, T., Islam, M.T. and Syvitski, J.P.M., (2018), Global river slope: A new geospatial dataset and global-scale analysis. *Journal of hydrology*, *563*, pp.1057-1067.

Dunn, F. E., S. E. Darby, R. J. Nicholls, S. Cohen, C. Zarfl, B.M. Fekete, (2019). **Projections of Declining Fluvial Sediment Delivery to Major Deltas Worldwide in Response to Climate Change and Anthropogenic Stress**. *Environmental Research Letters*, 14 (8), 084034.

Dunn E. F., R. J. Nicholls, S. E. Darby, S. Cohen, C. Zarfl, B. M. Fekete, (2018). **Projections of historical and 21st century fluvial sediment delivery to the Ganges-Brahmaputra-Meghna, Mahanadi, and Volta deltas**. *Science of The Total Environment*, 642, 105-116.

Dunne T, Mertes LAK, Meade RH, Richey JE, Forsberg B. 1998. Exchanges of sediment between the flood plain and channel of the Amazon River in Brazil. Geological Society of America Bulletin 110: 450–467.

Engelund, F., & Hansen, E. (1967). A monograph on sediment transport in alluvial streams. *Monografia*.

Fekete, B. M., A. Andreu, R. Argent, T. Avellán, C. Birkett, S. Caucci, S. Cohen, U. Looser, (2021). **Observations, Monitoring and Data Management**. *In J. J. Bogardi, J. Gupta, K. D. W. Nandalal, L. Salamé, R. R. P. van Nooijen, N. Kumar, … A. G. Kolechkina (Eds.), Handbook of Water Resources Management: Discourses, Concepts and Examples* (pp. 385–442).

Fofonova, V., Zhilyaev, I., Kraineva, M., Iakshina, D., Tananaev, N., Volkova, N., ... & Wiltshire, K. H. (2018). Features of the water temperature long-term observations on the Lena River at basin outlet. *Polarforschung*, *87*(2), 135-150.

Forbes D, Syvitski JPM, (1995). Paraglacial Coasts. In: C Woodruffe, RWG Carter (Eds.) *Coastal Evolution.* Cambridge University of Press, Cambridge, UK. Chapter 10: p. 373-424.

Gomez, B. (1991). Bedload Transport. *Earth-Science Reviews, 31*(2), 89-132.

Hackney, C.R., Darby, S.E., Parsons, D.R., Leyland, J., Best, J.L., Aalto, R., Nicholas, A.P. and Houseago, R.C., (2020). River bank instability from unsustainable sand mining in the lower Mekong River. *Nature Sustainability*, 3, 217–225. https://doi.org/10.1038/s41893-019-0455-3

Hatono, M., Yoshimura, K. Development of a global sediment dynamics model. *Prog Earth Planet Sci* 7, 59 (2020). https://doi.org/10.1186/s40645-020-00368-6

Islam, Md T. (2018). **Global Scale Bedload Flux Modeling.** *M.Sc Thesis, The University of Alabama.*

Kabir, M. A., Dutta, D., Hironaka, S., & Pang, A. (2012). Analysis of Bed Load Equations and River Bed Level Variations Using Basin-Scale Process-Based Modelling Approach. *Water Resources Management, 26*(5), 1143-1163.

Kettner, A. J., & Syvitski, J. P. M. (2008). HydroTrend v.3.0: A climate-driven hydrological transport model that simulates discharge and sediment load leaving a river system. *Computers & Geosciences, 34*(10), 1170-1183.

Lammers, R. W., & Bledsoe, B. P. (2018). Parsimonious sediment transport equations based on Bagnold's stream power approach. *Earth Surface Processes and Landforms*, *43*(1), 242-258.

Lehner, B, K. L. Verdin, and A. Jarvis. (2008). New Global Hydrography Derived from Spaceborne Elevation Data. *AGU EOS Transactions* 89, no. 10: 93–94.

Lehner, B., C. Reidy Liermann, C. Revenga, C. Vörösmarty, B. Fekete, P. Crouzet, P. Döll, M. Endejan, K. Frenken, J. Magome, C. Nilsson, J.C. Robertson, R. Rodel, N. Sindorf, and D. Wisser. (2011). High-resolution mapping of the world's reservoirs and dams for sustainable river-flow management. Frontiers in Ecology and the Environment 9 (9): 494-502.

Li, H.-Y., Tan, Z., Ma, H., Zhu, Z., Abeshu, G., Zhu, S., Cohen, S., Zhou, T., Xu, D., and Leung, L.-Y. R. (2021). A new large-scale suspended sediment model and its application over the United States. Hydrol. *Earth Syst. Sci. Discuss.* [preprint], https://doi.org/10.5194/hess-2021-491.

Li, L., Ni, J., Chang, F., Yue, Y., Frolova, N., Magritsky, D., ... & Walling, D. E. (2020). Global trends in water and sediment fluxes of the world's large rivers. *Science Bulletin*, *65*(1), 62-69.

Lin, P., Pan, M., Allen, G. H., de Moraes Frasson, R. P., Zeng, Z., Yamazaki, D., & Wood, E. F. (2020). Global estimates of reach-level bankfull river

width leveraging big data geospatial analysis. *Geophysical Research Letters*, 47, e2019GL086405. https://doi.org/10.1029/2019GL086405

Ma, H., Nittrouer, J. A., Naito, K., Fu, X., Zhang, Y., Moodie, A. J., & Parker, G. (2017). The exceptional sediment load of fine-grained dispersal systems: Example of the Yellow River, China. *Science advances*, 3(5), e1603114.

McKay, L., Bondelid, T., Dewald, T., Johnston, J., Moore, R., and Rea, A. (2012). *NHDPlus Version 2: User Guide*.

McCutcheon, S.C., Martin, J.L., Barnwell, T.O. Jr, 1993. Chapter 11: water quality. In: D.R. Maidment (Ed.) Handbook of Hydrology. McGraw Hill.

Meyer-Peter E. & Müller R. (1948). Formulas for bed-load transport. Paper presented at the 2nd Meeting of the International Association of Hydraulic Structures Research, Madrid.

Miara, A., Vörösmarty, C.J., Macknick, J.E., Tidwell, V.C., Fekete, B., Corsi, F., Newmark, R., (2018), Thermal pollution impacts on rivers and power supply in the Mississippi River watershed. *Environ. Res. Lett.* 13, 034033.

Milliman, J. D., & Farnsworth, K. L. (2011). River discharge to the coastal ocean: a global synthesis. *Cambridge University Press*.

Moragoda, N., S. Cohen, (2020). **Climate-induced Trends in Global Riverine Water Discharge and Suspended Sediment Dynamics in the 21st Century**. *Global and Planetary Change,* 191, 103199.

Morehead, M.D., Syvitski, J.P.M., Hutton, E.W.H., Peckham, S.D., (2003), Modeling the inter- annual and intra-annual variability in the flux of sediment in ungauged river basins. *Glob. Planet. Chang.* 39 (1/2), 95–110.

Montanher, O. C., Novo, E. M. L. D. M., & Souza Filho, E. E. D. (2018). Temporal trend of the suspended sediment transport of the Amazon River (1984–2016). *Hydrological Sciences Journal*, *63*(13-14), 1901-1912.

Overeem, I., Hudson, B., Syvitski, J. *et al.* (2017). Substantial export of suspended sediment to the global oceans from glacial erosion in Greenland. *Nature Geosci* 10, 859–863. https://doi.org/10.1038/ngeo3046

Parker, G. (1990). Surface-based bedload transport relation for gravel rivers. *Journal of Hydraulic Research*, 28(4), 417-436.

Peduzzi, P., (2014). Sand, rarer than one thinks. *Environmental Development,* 11, 208-218.

Rachold, A. Alabyan, H.-W. Hubberten, V. N. Korotaev & A. A. Zaitsev (1996) Sediment transport to the Laptev Sea–hydrology and geochemistry of the Lena River, Polar Research, 15:2, 183-196, DOI: 10.3402/polar.v15i2.6646

Recking, A. (2019). BedloadWeb User Manuel. 10.13140/RG.2.2.32856.34564/1

Syvitski, J.P., S. Cohen, A. Miara, J. Best, (2019). **River Temperature and the Thermal-Dynamic Transport of Sediment**. *Global and Planetary Change,* 178,168-183.

Syvitski, J. P. M., & Saito, Y. (2007). Morphodynamics of deltas under the influence of humans. *Global and Planetary Change*, 57(3-4), 261–282.

Syvitski JPM, Milliman JD, 2007, Geology, geography, and humans battle for dominance over the delivery of sediment to the coastal ocean. *Journal of Geology* 115: 1-19.

Syvitski, J. P. M., Vörösmarty, C. J., Kettner, A. J., & Green, P. (2005). Impact of humans on the flux of terrestrial sediment to the global coastal ocean. *Science*, 308(5720), 376-380.

Tananaev, N.I. & Anisimova, L.A. (2013): Evaluating the annual runoff of traction load on the rivers in the north of Siberia and the Far East.- Geogr. Nat. Resour. 34: 79-87.

Wisser, D., Frolking, S., Douglas, E., Fekete, B.M., Schuman, A.H., Vörösmarty, C.J. (2010). The significance of local water resources captured in small reservoirs for crop production—a global-scale analysis. *Journal of Hydrology*, 384, 264–275.

Wollheim, W. M., Vörösmarty, C. J., Bouwman, A. F., Green, P., Harrison, J., Linder, E., & Syvitski, J. P. (2008). Global N removal by freshwater aquatic systems using a spatially distributed, within - basin approach. *Global Biogeochemical Cycles*, 22(2).

Captions

Figure 1. WBMsed model sensitivity plots showing the regression between normalized [0,1] bedload at the modeled domain (91,659 grid-cells) and (a) discharge, (b) river slope, (c) river width, and (d) particle size.

Figure 2. River slope (top) and particle size (bottom) maps. Width of the lines indicates average river-reach discharge.

Figure 3. Average (1990-2019) predicted Qs (top) and Qb (bottom) in Mt/y. The width of the lines is indicative of average river-reach discharge. Note differences in color scheme scale.

Figure 4. Proportion of bedload flux from total sediment flux (a) map, (b) bedload latitudinal averages, (c) suspended load latitudinal averages, (d) bedload proportion latitudinal averages, and (d) histogram of all grid cells (Q>30 m3/s).

Figure 5. Boxplots of bedload proportion in river outlets to global oceans with average discharge greater than 30 m3/s (n = 2,067, draining 67% of continental land mass (excluding Antarctica)), 100 m3/s (n = 919, draining 60%), 500 m3/s

(n = 218, draining 50%), 1,000 m3/s (n = 114, draining 44%), 2,500 m3/s (n = 47, draining 37%), and 5,000 m3/s (n = 25, draining 33%). Black line within the box denotes the median, x denotes the mean and circles are outliers.

Figure 6. Mississippi/Missouri longitudinal profile (a) map, (b) bedload (kg/s), suspended load (kg/s) and bedload proportion (%), (c) river slope (-) and average bed-material grainsize (mm), and (d) relationship between river slope (-) and bedload proportion (%). Colored bars on (b) and (c) correspond to boxes in (a) and the satellite imagery panels. Green star in (b) is observed Qs from gage site USGS 07022000 Mississippi River at Thebes, IL (2550 kg/s); brown star is observed bedload from Nittrouer et al. (2008).

Figure 7. Lena/Vitim longitudinal profile (a) map, (b) bedload (kg/s), suspended load (kg/s) and bedload proportion (%), (c) river slope (-) and size-average bed-material grainsize (mm), and (d) relationship between river slope (-) and bedload proportion (%). Colored bars on (b) and (c) correspond to boxes in (a). Green star in (b) is average of reported SSF range at Kyusyr (11.8 to 21 Mt/yr; Are & Reimnitz, 2000); Brown star is observed bedload at Kusur GS reported by Fofonova et al. (2017).

Figure 8. Amazon/Marañón longitudinal profile (a) map, (b) bedload (kg/s), suspended load (kg/s) and bedload proportion (%), (c) river slope (-) and size-average bed-material grainsize (mm), and (d) relationship between river slope (-) and bedload proportion (%). Colored bar on (b) and (c) correspond to boxe in (a). Green star in (b) is a range of observed SSF at Óbidos summarized in Montanher et al. (2018).

Figure 9. Normalized [0,1] bedload proportion and elevation profiles along a normalized longitudinal profile for (a) Mississippi/Missouri, (b) Lena/Vitim, and (c) Amazon/Marañón.

Table 1. Summary statistics for all grid-cells with Q >30 m3/s, Qb > 1 kg/s (N = 91,659).

Table 2. Statistics for river outlets at 6 discharge filtering brackets. See Figure 6 caption for information about the number of outlets and landmass representation of each bracket. Bedload proportion Sum was calculated from bedload and total sediment Sum values (in italic).